of an influence by magnetic storm currents in the ionosphere. Such currents follow a diurnal cycle, reversing direction at a given location every 12 hours. There is a time-phase difference of about 7 hours between the two distributions. This is as might be expected in view of the different satellite headings and different latitudes at the sites used for the two sets of observations.

Conclusion

The data of Figs. 5, 6, and 7 suggest satellite-induced ionization effects at relatively short ranges from the satellite or within a few hundred kilometers. However, the data of Figs. 1, 2, 3, and 4 indicate satellite-related ionization effects from greater distances. As indicated in these figures, many satellite-related events appear to occur as much as 20 minutes before the time of passage of the satellite. Assuming a satellite velocity of 350 kilometers per minute, the satellite would be, therefore, at a distance of 7000 kilometers from the observer at the time of such events. Although mhd waves were mentioned as a mechanism in connection with the short range effects, this is only a speculative suggestion. More data are required to determine what mechanism or mechanisms may actually be responsible for both the short and longer distance effects and systematic high-power pulse-radar observations are being conducted at the OSURO for this purpose.

The Dielectric Microwave Resonator*

A. OKAYA† AND L. F. BARASH‡, MEMBER, IRE

Summary—**Pieces of single crystals of rutile show high Q resonances in the microwave range. A piece about $(1/7\,\lambda)^3$ has a Q as high as that of a metal-walled cavity at room temperature. Lowering the temperature increases both the Q and the resonant wavelength. Q's of 10^5 were seen at 4°K. A frequency equation of first- and second-order approximations was derived in terms of the dimensions and the anisotropic dielectric constant, ϵ', for rectangular parallelepiped resonators. Accurate values of anisotropic ϵ' were obtained.**

In the anisotropic medium there are two types of resonant modes, one of which has an outside E field similar to an electric multipole, and the other an outside magnetic field similar to a magnetic multipole. These two types of modes degenerate into one type if the dielectric is isotropic. Resonators were also made of ceramic rutile and strontium titanate, both of which had Q values of thousands. An extremely high unloaded Q, of the order of a million, was seen at 1.4°K on a KRS-5 (ThBr-ThI) single crystal at X band.

I. Introduction

METAL CAVITIES have long been used as microwave resonators, occasionally combined with dielectric materials. Dielectrics themselves have not been used in this way, but were considered only theoretically for use at high frequencies [2].

One can see that the surface between air and a dielectric will be a perfect reflector of microwaves if the angle of incidence is greater than the critical angle, $\theta_c = \sin^{-1} 1/\epsilon'^{1/2}$ where ϵ' is the imaginary part of electric susceptibility and is the dielectric constant. Hence, a piece of dielectric in air may be a microwave resonator if the microwave loss is small.

It was found that a piece of rutile, *et al.*, fulfilled the conditions for such a resonator and that the unloaded Q of a rutile resonator was as high as, or higher than, that of a metal-walled cavity [1]. The high Q results from very small dielectric losses and no wall losses in the resonator. The resonant frequency is determined by the ϵ', the dimensions, and the shape of a resonator.

This resonance effect in rutile found an effective use in electron paramagnetic resonance experiments [3] on Fe^{3+} and Cr^{3+} in rutile single crystals. The sensitivity of EPR was enormously increased by this resonance phenomenon, and resonances of Fe^{3+} were observed from 2 kMc to 120 kMc with ease. Furthermore, not only Ti^{3+}, but the spectra of sparsely populated color centers and vacancies [4] in a "pure" rutile single crystal (impurity less 0.001 per cent) were also seen.

The large zero-magnetic-field splitting of Fe^{3+} (43.3 kMc and 81.3 kMc) and Cr^{3+} (43 kMc), the fairly long relaxation times, and the microwave resonant characteristics make rutile quite useful as a maser material, especially in the millimeter wave region. (Several rutile millimeter and centimeter masers have been made recently by groups at CRL [5], M.I.T. [6], and RCA [7].)

* Received January 11, 1962; revised manuscript received May 2, 1962. The work reported here was supported jointly by the U. S. Army Signal Corps, the Office of Naval Research, and the Air Force Office of Scientific Research. Parts of this work were reported in the Columbia Radiation Laboratory Quarterly Progress Reports [1], and the Proceedings of the IRE [11].

† IBM Communications Systems Center, Rockville, Md. Formerly with Columbia Radiation Laboratory, Columbia University, New York, N. Y.

‡ Formerly with Columbia Radiation Laboratory, Columbia University, New York, N. Y.

For these reasons and for general interest, the study of microwave field configurations and the characteristics of dielectric resonators was undertaken.

A first-order approximation for the frequency equation of modes in anisotropic media for rectangular parallelepipeds was derived, assuming perfect reflection at the resonator surface. This was compared with experimental results. Modes were identified, and fairly good agreement of frequencies at high modes was obtained. Extension of the first-order approximation to the more general case of anisotropic permeability μ and the dielectric constant ϵ' is treated in Appendix I. For the second-order approximation, more realistic boundary conditions were considered. The results were applied to the fundamental modes to obtain accurate solutions for frequency in terms of the dimensions and dielectric constant. Using measured resonant frequency, the anisotropic ϵ' was calculated accurately by this equation. Finally, the use of dielectric resonators in microwave filter circuits is discussed.

II. First-Order Approximation of the Resonant Frequency Equation

Assuming that the boundary coincides with a node or antinode of either the electric or magnetic field, we confine our discussion to dielectric slabs of rectangular cross section and solve Maxwell's equation for the dielectrics. It will be shown in Section III that this assumption is valid if the resonator dimension is larger than the effective wavelength in the crystal, $\lambda/\epsilon'^{1/2}$. We also assume that $\mu=1$, both inside and outside the dielectric, and that the dielectric constants along the three axes, taken parallel to the resonator surfaces, are ϵ_x', ϵ_y', and ϵ_z', respectively, (see Fig. 1). As the solutions of Maxwell equations

$$\nabla \times \boldsymbol{E} = -\dot{\boldsymbol{H}},$$
$$\nabla \times \boldsymbol{H} = \epsilon \dot{\boldsymbol{E}}, \tag{1}$$

we assume an electric field of the following form

$$E_x = A_x \begin{matrix}\cos\\ \sin\end{matrix} \xi x \begin{matrix}\cos\\ \sin\end{matrix} \eta y \begin{matrix}\sin\\ \cos\end{matrix} \zeta z e^{i\omega t},$$

$$E_y = A_y \begin{matrix}\sin\\ \cos\end{matrix} \xi x \begin{matrix}\sin\\ \cos\end{matrix} \eta y \begin{matrix}\sin\\ \cos\end{matrix} \zeta z e^{i\omega t},$$

$$E_z = A_z \begin{matrix}\sin\\ \cos\end{matrix} \xi x \begin{matrix}\cos\\ \sin\end{matrix} \eta y \begin{matrix}\cos\\ \sin\end{matrix} \zeta z e^{i\omega t}. \tag{2}$$

Hereafter, for convenience, ϵ' will be written as ϵ, where the boundary conditions on the surface are already taken into account.

Then we take the following three cases which are applicable to rutile:

$$\text{Case I} \quad \epsilon_z = \epsilon_\parallel \qquad \epsilon_x = \epsilon_y = \epsilon_\perp,$$
$$\text{Case II} \quad \epsilon_x = \epsilon_\parallel \qquad \epsilon_y = \epsilon_z = \epsilon_\perp,$$
$$\text{Case III} \quad \epsilon_y = \epsilon_\parallel \qquad \epsilon_x = \epsilon_z = \epsilon_\perp, \tag{3}$$

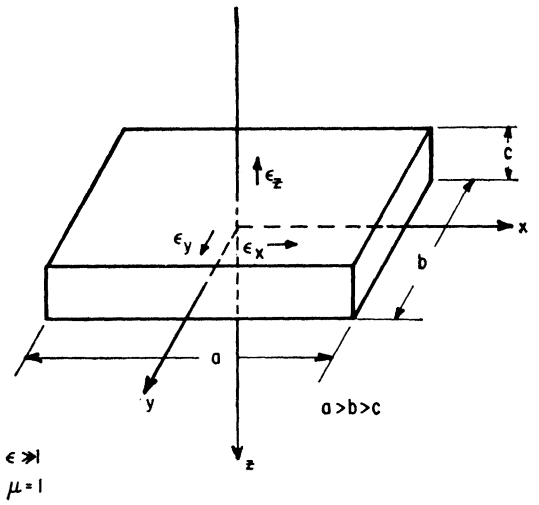

Fig. 1—Rutile dielectric microwave resonator.

where $\epsilon_\parallel$ and $\epsilon_\perp$ are the dielectric constants parallel and perpendicular to the optic axis. Dimensions a, b, and c are the crystal dimensions along the x, y, and z axes, as shown in Fig. 1. From the linear equations, which will be reduced from (1) and (2) and after considering the conditions of (3), we have solutions which satisfy the condition of nonzero E_x, E_y, and E_z field.

$$\text{Case I} \quad \left(\frac{2}{\lambda}\right)^2 = \frac{1}{\epsilon_\perp}\left[\left(\frac{l}{a}\right)^2 + \left(\frac{m}{b}\right)^2 + \left(\frac{n}{c}\right)^2\right],$$
$$\left(\frac{2}{\lambda}\right)^2 = \frac{1}{\epsilon_\parallel}\left[\left(\frac{l}{a}\right)^2 + \left(\frac{m}{b}\right)^2\right] + \frac{1}{\epsilon_\perp}\left(\frac{n}{c}\right)^2,$$

$$\text{Case II} \quad \left(\frac{2}{\lambda}\right)^2 = \frac{1}{\epsilon_\perp}\left[\left(\frac{l}{a}\right)^2 + \left(\frac{m}{b}\right)^2 + \left(\frac{n}{c}\right)^2\right],$$
$$\left(\frac{2}{\lambda}\right)^2 = \frac{1}{\epsilon_\perp}\left(\frac{l}{a}\right)^2 + \frac{1}{\epsilon_\parallel}\left[\left(\frac{m}{b}\right)^2 + \left(\frac{n}{c}\right)^2\right],$$

$$\text{Case III} \quad \left(\frac{2}{\lambda}\right)^2 = \frac{1}{\epsilon_\perp}\left[\left(\frac{l}{a}\right)^2 + \left(\frac{m}{b}\right)^2 + \left(\frac{n}{c}\right)^2\right],$$
$$\left(\frac{2}{\lambda}\right)^2 = \frac{1}{\epsilon_\parallel}\left[\left(\frac{l}{a}\right)^2 + \left(\frac{n}{c}\right)^2\right] + \frac{1}{\epsilon_\perp}\left(\frac{m}{b}\right)^2. \tag{4}$$

where

$$\xi = \frac{l}{a}\pi, \quad \eta = \frac{m}{b}\pi, \quad \zeta = \frac{n}{c}\pi$$

and l, m and n are integers.

There are two solutions for each case. The first is the same for each of the three cases and results from the isotropy of μ. The second solution, which is different for the three cases, results from the anisotropy of ϵ. Exactly the same results are obtained when the equation for the magnetic field is solved. Detailed boundary conditions are discussed in Section III. In Cases I and II, (4) is about 25 per cent in error for the lowest modes but becomes increasingly accurate for higher modes where the assumption of nodes or antinodes at the boundaries becomes more realistic. The above solutions, however, are accurate enough for identification of the modes and

for rough estimates of frequency. The solutions for the general case of completely anisotropic μ and ϵ are derived in Appendix I, and one can deduce (4) from those results as a special case. For a completely isotropic medium, there is a single-frequency equation and, therefore, only half as many modes.

III. Boundary Conditions

The boundaries of the dielectric resonator could be interpreted as follows. Suppose we have an isotropic dielectric sheet of infinite extent whose thickness in the z direction is c, as shown in Fig. 2. We shall, for simplicity, discuss this two-dimensional case first. The E field parallel to the resonator surface should be continuous across its boundary. Hence

$$E_{ix} = E_{ox}, \tag{5}$$

where E_{ix} and E_{ox} are the inside and outside electric fields parallel to the surface, respectively. Also,

$$\nabla \times \boldsymbol{E} = \dot{\boldsymbol{B}},$$
$$\nabla \cdot \boldsymbol{B} = 0. \tag{6}$$

Hence, $\partial E_x/\partial z = \text{constant}$.

Let us assume that, at resonant condition, the standing wave of an electric field has sinusoidal variation inside a resonator and decays exponentially outside it.

The detailed discussions of Section IV will explain that the exponential decay is a good approximation in the space close to the surface. The x component of the electric field will be given by

$$\text{Inside:} \quad E_{xi} = e_{xi} \cos \zeta_i z e^{i\omega t},$$
$$\text{Outside:} \quad E_{xo} = e_{xo} e^{-\zeta_o z} e^{i\omega t}, \tag{7}$$

where ω is the resonant angular frequency and ζ_i and ζ_o are the propagation constants along the z direction inside and outside, respectively.

From (5), (6), and (7) we have

$$\zeta_i \tan \zeta_i \frac{c}{2} = +\zeta_o, \tag{8}$$

here, c is the thickness of the resonator. Then e_{xi} is a function of the propagation constant ρ along the x direction, *i.e.*,

$$e_{xi} = e_i e^{\rho_i x_i}. \tag{9}$$

The field outside, but immediately adjacent to the surface, has to equal the field just inside and has to have the same maximum and minimum points. Therefore, the propagation constants inside and outside a resonator should be the same and $\rho_i = \rho_o$.

On the other hand, the propagation constants must satisfy the following equation [8]:

$$\rho_i^2 + \zeta_o^2 = \beta^2 \text{ outside}, \tag{10a}$$
$$\rho_i^2 + \zeta_i^2 = \epsilon\beta^2 \text{ inside}, \tag{10b}$$

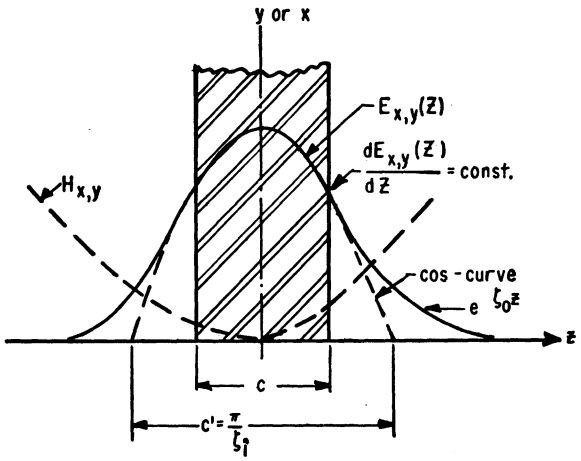

Fig. 2—Field configuration along the z axis.

where

$$\beta = \frac{2\pi}{\lambda} = \frac{\omega}{c} = \text{intrinsic phase constant.}$$

Therefore, $\zeta_i \gg \zeta_o$ for large ϵ.

Putting (10) into (8) we have

$$\left(\frac{c\zeta_i}{2}\right)^2 \tan^2 \frac{c\zeta_i}{2} = (\beta^2 - \rho_i^2)\left(\frac{c}{2}\right)^2, \tag{11}$$

where ρ_i is imaginary [as we expected from (9)]. The transverse propagation constant ρ_i is of the order of $2\sqrt{\epsilon}/\lambda$ and $\rho_i \gg \beta$. Then the right side of (11) is rewritten,

$$(\beta^2 - \rho_i^2)\left(\frac{c}{2}\right)^2 \simeq -\left(\frac{c\rho_i}{2}\right)^2 \simeq \left(\frac{c\sqrt{\epsilon}}{\lambda}\right)^2, \tag{12}$$

where $\lambda/\sqrt{\epsilon}$ is the effective wavelength inside the dielectric. Combining (12) and (11) we can see that if the thickness c is much greater than the effective wavelength in the medium $\lambda/\sqrt{\epsilon}$, then $c\zeta_i/2$ approaches $\pi/2$, and therefore $(c/\pi)\zeta_i$ approaches unity. This means that $\pi/\zeta_i = c$ will be a good approximation if $c \gg \lambda/\sqrt{\epsilon}$.

This explains that if c is much greater than $\lambda/\sqrt{\epsilon}$, π/ζ_i is very nearly equal to c, then the boundary surface can be treated as a node of the standing waves inside the medium. This is why the first-order approximation for the frequency equation, as treated in Section II, fits well for the higher order modes. The further physical meaning of these equations can be more clearly understood from Fig. 2. If the resonator is thin, as compared with $\lambda/\sqrt{\epsilon}$, the effective wavelength in the dielectrics, then more E field extends outside the resonator.

IV. A Second-Order Approximation for the H Mode

We will now confine the problem to the fundamental H mode $TM_{11\delta}$, and discuss the details of the three-dimensional field inside a resonator for the three different cases of (3).

$TM_{\|\delta}$ means that the E field varies a half cycle along the x and y axes, and varies only the fraction $\delta=(c/\pi)\zeta_i$ of the sine wave along the z axis inside a resonator. The E field inside the resonator can be written in the following form:

$$E_{xi} = A_x(z)\cos\xi x \sin\eta y e^{i\omega t},$$
$$E_{yi} = A_y(z)\sin\xi x\cos\eta y e^{i\omega t},$$
$$E_{zi} = 0. \tag{13}$$

After substituting the above equation into Maxwell's equation (1) we have

$$\frac{d^2A_x}{dz^2} + (\epsilon_x\beta^2 - \eta^2)A_x + \xi\eta A_y = 0,$$
$$\frac{d^2A_y}{dz^2} + (\epsilon_y\beta^2 - \xi^2)A_y + \xi\eta A_x = 0, \tag{14}$$
$$\xi\frac{dA_x}{dz} = -\eta\frac{dA_y}{dz}.$$

One can express a solution by means of two orthogonal modes with different propagation constants ζ_{i-} and ζ_{i+} in the following form:

$$A_x = C_-\sin\alpha_i e^{i\zeta_{i-}z} + C_+\cos\alpha_i e^{i\zeta_{i+}z},$$
$$A_y = C_-\cos\alpha_i e^{i\zeta_{i-}z} - C_+\sin\alpha_i e^{i\zeta_{i+}z}. \tag{15}$$

Here, α_i is the angle between the principal axis of the orthogonal mode and the x and y axes. Then the propagation constants $\zeta_{i\pm}$ along the z axis should satisfy the relation

$$\zeta_{i\pm}^2 = \tfrac{1}{2}\left[\beta^2(\epsilon_x+\epsilon_y) - (\xi^2+\eta^2) \pm \left\{[\beta^2(\epsilon_x-\epsilon_y) - (\xi^2-\eta^2)]^2 + 4\xi^2\eta^2\right\}^{1/2}\right], \tag{16}$$

and the angle α_i should satisfy

$$\tan\alpha_i = -\frac{1}{2\xi\eta}\left\{[\beta^2(\epsilon_y-\epsilon_x) + (\eta^2-\xi^2)] + [\{\beta^2(\epsilon_x-\epsilon_y) - (\xi^2-\eta^2)^2 + 4\xi^2\eta^2]^{1/2}\right\}, \tag{17}$$

where $\xi=\pi l/a$, $\eta=\pi m/b$ are propagation constants along the x and y axes and l and m are integers.

For the three cases defined in Section II, (16) and (17) become:

Case I.

$$(\zeta_{i-}/\pi)^2 = \left(\frac{2}{\lambda}\right)^2\epsilon_\perp - \left[\left(\frac{l}{a}\right)^2 + \left(\frac{m}{b}\right)^2\right], \tag{18a}$$

where ζ_{i+} is eliminated from the solutions, because it does not satisfy the boundary conditions as we can see from (7);

$$\tan\alpha_i = -\frac{\eta}{\xi} = -\frac{ma}{lb}. \tag{18b}$$

Case II.

$$(\zeta_{i\pm}/\pi)^2 = \frac{1}{2}\left[\left(\frac{2}{\lambda}\right)^2(\epsilon_\| + \epsilon_\perp) - \left(\frac{l}{a}\right)^2 - \left(\frac{m}{b}\right)^2 \pm \left\{\left[\left(\frac{2}{\lambda}\right)^2(\epsilon_\| - \epsilon_\perp) + \left(\frac{l}{a}\right)^2 - \left(\frac{m}{b}\right)^2\right]^2 + 4\left(\frac{lm}{ab}\right)^2\right\}^{1/2}\right], \tag{19a}$$

$$\tan\alpha_i = -\frac{ab}{2lm}\left[\left(\frac{2}{\lambda}\right)^2(\epsilon_\perp - \epsilon_\|) - \left(\frac{l}{a}\right)^2 + \left(\frac{m}{b}\right)^2 + \left\{\left[\left(\frac{2}{\lambda}\right)^2(\epsilon_\| - \epsilon_\perp) + \left(\frac{l}{a}\right)^2 - \left(\frac{m}{b}\right)^2\right]^2 + 4\left(\frac{lm}{ab}\right)^2\right\}^{1/2}\right]. \tag{19b}$$

Case III.

$$(\zeta_{i\pm}/\pi)^2 = \frac{1}{2}\left[\left(\frac{2}{\lambda}\right)^2(\epsilon_\| + \epsilon_\perp) - \left(\frac{l}{a}\right)^2 - \left(\frac{m}{b}\right)^2 \pm \left\{\left[\left(\frac{2}{\lambda}\right)^2(\epsilon_\perp - \epsilon_\|) + \left(\frac{l}{a}\right)^2 - \left(\frac{m}{b}\right)^2\right]^2 + 4\left(\frac{lm}{ab}\right)^2\right\}^{1/2}\right], \tag{20a}$$

$$\tan\alpha_i = \frac{-ab}{2lm}\left[\left(\frac{2}{\lambda}\right)^2(\epsilon_\| - \epsilon_\perp) - \left(\frac{l}{a}\right)^2 + \left(\frac{m}{b}\right)^2 + \left\{\left[\left(\frac{2}{\lambda}\right)^2(\epsilon_\perp - \epsilon_\|) + \left(\frac{l}{a}\right)^2 - \left(\frac{m}{b}\right)^2\right]^2 + 4\left(\frac{lm}{ab}\right)^2\right\}^{1/2}\right]. \tag{20b}$$

Now let the field outside the resonator be such that the inside and outside fields are matched on the $x-y$ plane at $z=\pm c/2$.

Immediately outside the resonator the E field must have the same periodicity as the field just inside the resonator. Hence, we express the E field in the form

$$E_{xo} = B_x(z)\cos\xi x\sin\eta y e^{i\omega t},$$
$$E_{yo} = B_y(z)\sin\xi x\cos\eta y e^{i\omega t},$$
$$E_{zo} = 0. \tag{21}$$

Note that these equations are true only very close to the boundary.

The wave equation for the outside field is the same as (14) except for $\epsilon=1$, and its solutions are

$$B_x = D_- \sin \alpha_o e^{i\zeta_{o-}z} + D_+ \cos \alpha_o e^{i\zeta_{o+}z}$$
$$B_y = D_- \cos \alpha_o e^{i\zeta_{o-}z} - D_+ \sin \alpha_o e^{i\zeta_{o+}z}, \tag{22}$$

where

$$(\zeta_{o-}/\pi)^2 = \left(\frac{2}{\lambda}\right)^2 - \left[\left(\frac{l}{a}\right)^2 + \left(\frac{m}{b}\right)^2\right],$$
$$(\zeta_{o+}/\pi)^2 = \left(\frac{2}{\lambda}\right)^2, \tag{23}$$
$$\tan \alpha_o = -\frac{\eta}{\xi} = -\frac{ma}{lb}.$$

$i\zeta_{o-}$ is real and shows an exponentially damped wave outside of the resonator. On the other hand, $i\zeta_{o+}$ is imaginary and shows propagation without attenuation.

From (6) we have the boundary condition

$$A_x = B_x\big|_{z=c/2} \qquad A_y = B_y\big|_{z=c/2}$$
$$\frac{\partial A_x}{\partial z} = \frac{\partial B_x}{\partial z}\bigg|_{z=c/2} \qquad \frac{\partial A_y}{\partial z} = \frac{\partial B_y}{\partial z}\bigg|_{z=c/2}. \tag{24}$$

Substituting (15) and (22) into (24), we have four linear equations for the C's and D's. To have a nonzero solution of C's and D's, the determinant derived from them must be equal to zero. After much painstaking algebra assuming

$$\left|\frac{\zeta_{o+}}{\zeta_{o-}}\right|^2 \simeq \frac{\left(\frac{2}{\lambda}\right)^2}{\left(\frac{l}{a}\right)^2 + \left(\frac{m}{b}\right)^2} \simeq \frac{1}{\epsilon} \simeq 0,$$

we have

$$\zeta_{o-}\left(\alpha\zeta_{i-}\tan\frac{c}{2}\zeta_{i-} + \beta\zeta_{i+}\tan\frac{c}{2}\zeta_{i+}\right)$$
$$\simeq \gamma\zeta_{i+}\zeta_{i-}\tan\frac{c}{2}\zeta_{i+}\tan\frac{c}{2}\zeta_{i-}, \tag{25}$$

where

$$\alpha = \sin^2(\alpha_i - \alpha_o),$$
$$\beta = \cos^2(\alpha_i - \alpha_o),$$
$$\gamma = 1.$$

For Case I, (25) is much simpler and becomes

$$\zeta_{o-} = \zeta_{i-}\tan\zeta_{i-}\frac{c}{2}. \tag{26}$$

Of course this result agrees with (14) of the two-dimensional case, as one expected.

Comparison with the experimental results will be discussed in Section VII.

V. A Second-Order Approximation for the E Mode

There is another set of modes which also satisfies the boundary conditions. In this case, the roles of E and H are interchanged from the H-mode case and the outside field is similar to an electric dipole. Hence, we call this case the E or TE mode. One can see that the field configuration inside the resonator is similar to the rectangular metal-wall cavity. The fundamental mode is called the $TE_{11\delta}$ for reasons analogous to the TE_{111} case. The calculations are similar to the H-mode case and are carried out in a similar way.

For the fundamental $TE_{11\delta}$ mode, we assume the H field, in analogy to (13), is of the form

$$H_{xi} = L_x(z)\cos\xi x \sin\eta y e^{i\omega t},$$
$$H_{yi} = L_y(z)\sin\xi x \cos\eta y e^{i\omega t},$$
$$H_{zi} = 0, \tag{27}$$

where

$$L_x = (M_- \cos\alpha_i \cos\zeta_{i-}z + M_+ \sin\alpha_i \cos\zeta_{i+}z)$$
$$L_y = (M_- \sin\alpha_i \cos\zeta_{i-}z - M_+ \cos\alpha_i \cos\zeta_{i+}z). \tag{28}$$

The solutions for the ζ_i and the angle α_i for the three cases are:

Case I.

$$(\zeta_{i-}/\pi)^2 = \epsilon_\perp\left(\frac{2}{\lambda}\right)^2 - \frac{\epsilon_\perp}{\epsilon_\parallel}\left[\left(\frac{l}{a}\right)^2 + \left(\frac{m}{b}\right)^2\right],$$

or

$$(2/\lambda)^2 = \frac{1}{\epsilon_\parallel}\left[\left(\frac{l}{a}\right)^2 + \left(\frac{m}{b}\right)^2\right] + \frac{1}{\epsilon_\perp}(\zeta_{i-}/\pi)^2,$$
$$(\zeta_{i+}/\pi)^2 = \epsilon_\perp\left(\frac{2}{\lambda}\right)^2,$$
$$\tan\alpha_i = -\frac{\eta}{\xi} = -\frac{ma}{lb}. \tag{29a}$$

Case II.

$$(\zeta_{i\pm}/\pi)^2 = \frac{1}{2}\left\{(\epsilon_\perp + \epsilon_\parallel)\left(\frac{2}{\lambda}\right)^2 - \left(\frac{m}{b}\right)^2 - \frac{\epsilon_\parallel}{\epsilon_\perp}\left(\frac{l}{a}\right)^2 \pm \left[\left\{\left(\frac{m}{b}\right)^2 - \frac{\epsilon_\parallel}{\epsilon_\perp}\left(\frac{l}{a}\right)^2 + \left(\frac{2}{\lambda}\right)^2(\epsilon_\perp - \epsilon_\parallel)\right\}^2 + \frac{4\epsilon_\parallel}{\epsilon_\perp}\left(\frac{lm}{ab}\right)^2\right]^{1/2}\right\}$$

$$\tan\alpha_i = \frac{1}{2}\frac{ab}{lm}\left\{\frac{\epsilon_\parallel}{\epsilon_\perp}\left(\frac{l}{a}\right)^2 - \left(\frac{m}{b}\right)^2 + \left(\frac{2}{\lambda}\right)^2(\epsilon_\parallel - \epsilon_\perp) - \left[\left\{\frac{\epsilon_\parallel}{\epsilon_\perp}\left(\frac{l}{a}\right)^2 - \left(\frac{m}{b}\right)^2 + \left(\frac{2}{\lambda}\right)^2(\epsilon_\parallel - \epsilon_\perp)\right\}^2 + \frac{4\epsilon_\parallel}{\epsilon_\perp}\left(\frac{lm}{ab}\right)^2\right]^{1/2}\right\}. \tag{29b}$$

Case III.

$$(\zeta_{i\pm}/\pi)^2 = \frac{1}{2}\left\{(\epsilon_\perp + \epsilon_\parallel)\left(\frac{2}{\lambda}\right)^2 - \frac{\epsilon_\parallel}{\epsilon_\perp}\left(\frac{m}{b}\right)^2 - \left(\frac{l}{a}\right)^2 \pm \left[\left\{\frac{\epsilon_\parallel}{\epsilon_\perp}\left(\frac{m}{b}\right)^2 - \left(\frac{l}{a}\right)^2 + \left(\frac{2}{\lambda}\right)^2(\epsilon_\parallel - \epsilon_\perp)\right\}^2 + \frac{4\epsilon_\parallel}{\epsilon_\perp}\left(\frac{lm}{ab}\right)^2\right]^{1/2}\right\}$$

$$\tan \alpha_i = \frac{1}{2}\frac{ab}{lm}\left\{\left(\frac{l}{a}\right)^2 - \frac{\epsilon_\parallel}{\epsilon_\perp}\left(\frac{m}{b}\right)^2 + \left(\frac{2}{\lambda}\right)^2(\epsilon_\perp - \epsilon_\parallel) - \left[\left\{\left(\frac{l}{a}\right)^2 - \frac{\epsilon_\parallel}{\epsilon_\perp}\left(\frac{m}{b}\right)^2 + \left(\frac{2}{\lambda}\right)^2(\epsilon_\perp - \epsilon_\parallel)\right\}^2 + 4\frac{\epsilon_\parallel}{\epsilon_\perp}\left(\frac{lm}{ab}\right)^2\right]^{1/2}\right\}. \quad (29c)$$

Then, using boundary conditions analogous to (24) and assuming the outside field is the same as (22) except that the E and H fields are interchanged, we have a boundary equation of the same form as (25), but with the following coefficients:

Case II.

$$\alpha = (\epsilon_\perp \sin\alpha_i \sin\alpha_o - \epsilon_\parallel \cos\alpha_i \cos\alpha_o)\cdot(\sin\alpha_i \sin\alpha_o - \cos\alpha_i \cos\alpha_o),$$
$$\beta = (\epsilon_\parallel \cos\alpha_i \cos\alpha_o + \epsilon_\perp \sin\alpha_i \cos\alpha_o)\cdot(\cos\alpha_i \sin\alpha_o + \sin\alpha_i \cos\alpha_o),$$
$$\gamma = \epsilon_\parallel \cos^2\alpha_i + \epsilon_\perp \sin^2\alpha_i. \quad (30)$$

VI. Physical Picture of the Field

Let us consider the $TM_{11\delta}$ mode of Case I. The propagation constants along the z axis for inside and outside fields are given by (18) and (23). For Case I, $\alpha_i = \alpha_o$ and (14) and (15), we have

$$\frac{C_+}{C_-} = \frac{\zeta_{i-}(\xi \sin\alpha_i - \eta\cos\alpha_i)}{\zeta_{i+}(\eta \sin\alpha_i + \xi\cos\alpha_i)} e^{i(\zeta_{i-}-\zeta_{i+})z}$$

but since $\tan\alpha_i = -\eta/\xi$, we have $C_+ = 0$. Similarly, for the outside field,

$$\frac{D_+}{D_-} = \frac{\zeta_{o-}(\xi \sin\alpha_o - \eta\cos\alpha_o)}{\zeta_{o+}(\eta \sin\alpha_o - \xi\cos\alpha_o)} e^{i(\zeta_{o-}-\zeta_{o+})z}.$$

Hence $D_+ = 0$, also. Therefore, only the C_- inside field couples to the D_- outside field, the attenuated wave, and not to the propagation wave D_+. On the other hand, in Cases II and III the situation becomes more complicated because of the anisotropy in the x-y plane. Both the C_- and C_+ waves of different propagation constants couple to the outside attenuation D_- wave and the propagation D_+ wave. An elliptically polarized wave is excited inside the resonator. Larger anisotropy induces more excitation of the propagation D_+ wave outside the resonator because $(\alpha_i - \alpha_o)$ becomes larger.

Coupling schemes of the resonator as a whole can be classified in the following two cases. The first is the coupling of the inside resonator field to the outside free-space field or to the waveguide field via the radiation field (dipole field, etc.) of the resonator. Hence, the coupling of this case depends upon both the coupling between the inside resonator field and the radiation field and the coupling between the radiation field and the free-space field. The first coupling is due to the perpendicular component of the Poynting vector on the resonator surface, which will be induced by a) distortion of the basic mode field and b) the presence of local higher-order modes. The second is the coupling of the inside field directly to the outside field by the C_+ and propagation D_+ modes. Let us consider the coupling of the dipole radiation field to the outside free-space field.

In the case of a magnetic dipole, the radiation impedance [9] of a loop in free space is given by

$$R_E = 7.9 \times 10^2 \left(\frac{R_1}{\lambda}\right)^2 \text{ ohms.} \quad (31a)$$

In our case, the radius of the loop R_1 corresponds to the resonator dimensions. For example, a rutile resonator measuring $0.123 \times 0.247 \times 0.470$ inches has a resonant wavelength of 6.83 cm. Then we have

$$R_H \cong 75 \text{ ohms.}$$

This impedance is about the same order of magnitude as free-space or waveguide impedance. On the other hand, the E dipole impedance is expressed as [9]

$$R_E \cong 3 \times 10^{-27}\left(\frac{\lambda}{R_1}\right)^4 \text{ ohms.} \quad (31b)$$

This is a very small number which makes coupling to free space almost impossible.

The exact calculation of the outside radiation field is quite complicated and is beyond the scope of our discussion in this paper. However, one can draw a picture of fields for either the Case I or isotropic resonator, depending upon the following statements:

a) Only a monotonically decreasing mode D_- exists at the outside of the resonator. It will be transferred smoothly to the outside dipole field.
b) The size of a resonator is quite small compared to the wavelength; hence, a resonator can be considered as nearly a point source radiator.
c) The direction of the E or H field at the origin of the radiator should be parallel to the z axis because of the boundary condition.

For these reasons, one can conclude that the field is nearly a dipole E or H field, as shown in Fig. 3. On the other hand, the radiation fields of higher modes are quite complicated but can be understood by comparison to the radiation pattern of a multipole antenna, which is somewhat similar to that case.

If the nonattenuating mode, which is due to the D_+

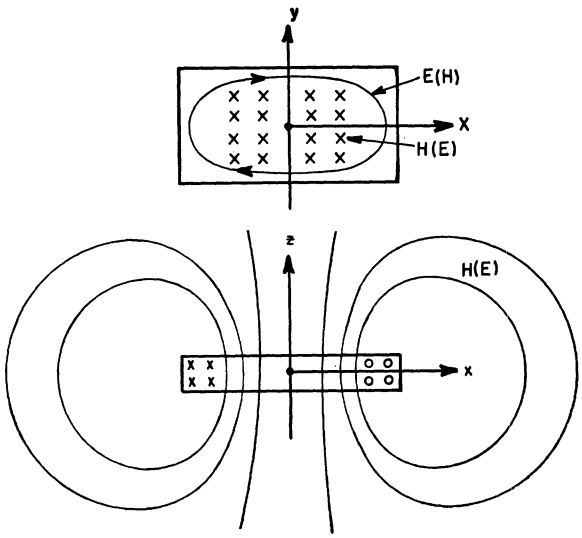

Fig. 3—Dipole radiation field of a resonator which resonates at fundamental anode.

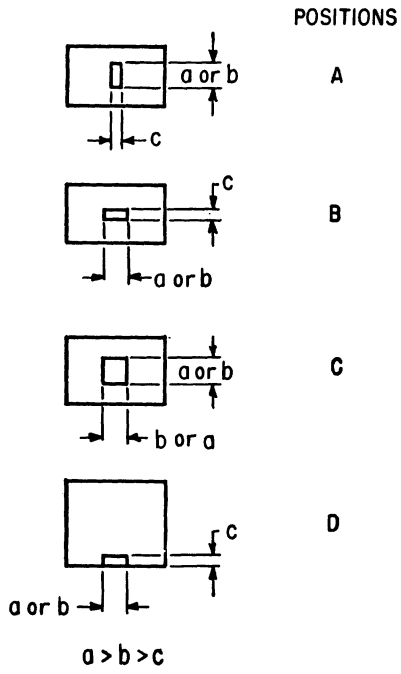

Fig. 4—Variable position of a resonator in the waveguide.

term, is superimposed on the above mentioned radiation mode, the situation becomes more complicated. This situation was observed as a change of coupling of a resonator when the Case II and Case III resonators in position A in Fig. 4 were rotated about the z axis. Other aspects of the resonator, such as Q values, will be discussed in another paper [12].

VII. Experimental Results

Experimental verification of the theory and accurate measurement of the dielectric constant ϵ, particularly in single crystal rutile, were made. The measurements of $\epsilon_{\|}$ in an anisotropic medium, such as rutile in the microwave region, are not reliable if one uses the conventional techniques. If the wave travels several wavelengths in the medium, the polarization plane of the incoming wave rotates about the direction of propagation and also changes its feature so that the effective path length is much greater than the physical length. This is especially important for the case in which the optical axis is perpendicular to the direction of propagation.

Before discussing the experimental results, the experimental procedure will be described. A piece of dielectric of known dimensions, resonant at microwave frequencies, was placed in a waveguide and supported in polyfoam. This polyfoam support had negligible loss and a dielectric constant very close to unity so that it did not disturb the fields surrounding the resonator.

The resonator was well isolated from both generator and detector by attenuators. The coupling of the resonator was adjusted by changing its orientation in the waveguide, about which more will be said later. It was also kept as far from the waveguide walls as possible to avoid distortion of the radiation field, and to compare with theoretical results based on a dielectric resonator in free space. As a check, the resonators were put in an oversized waveguide, or between waveguide horns. Only small frequency differences for either case were observed. The set-up is shown in Fig. 5(a). Crystal detectors #1 and #2 were used to monitor the reflected and transmitted power. The standing-wave detector was used to check the matching at resonance.

Fig. 5(b) shows the set-up used to measure the temperature effect on ϵ. One might expect a large standing wave to be caused by the shorting plunger, but in the experiments the QL of the resonators was so much higher than that of the standing waves due to the short that the two were easily distinguishable. The short served as a tuner to help match the resonator, whose position was fixed in the low temperature bath. This system was used at frequencies from 8 to 40 kMc and at temperatures from room temperature down to 78°K. At liquid helium temperatures, the set-up shown in Fig. 5(c) was used for frequencies below 8 kMc. ϵ vs temperature curves for rutile and $SrTiO_3$ are shown in Fig. 6.

For the Q measurements, detector #2 and an attenuator in Fig. 5(a) were replaced by a sliding short. The crystal resonator was critically coupled by adjusting the short, and the Q_o was measured at this point. The reflected wave from the crystal resonator was observed at detector #1. The position of the crystal resonator in the waveguide for maximum coupling was more or less opposite for the E and H modes so that the two types of modes were distinguished in this way. One can observe a variety of absorption or reflection patterns due to E or H mode resonance for high-order modes.

Sometimes our Q measurements were inaccurate because the waveguide wall, which induces skin loss, was not far enough away from the crystal resonator.

The rutile resonators were cut from single-crystal boules, which were optically oriented to an accuracy of

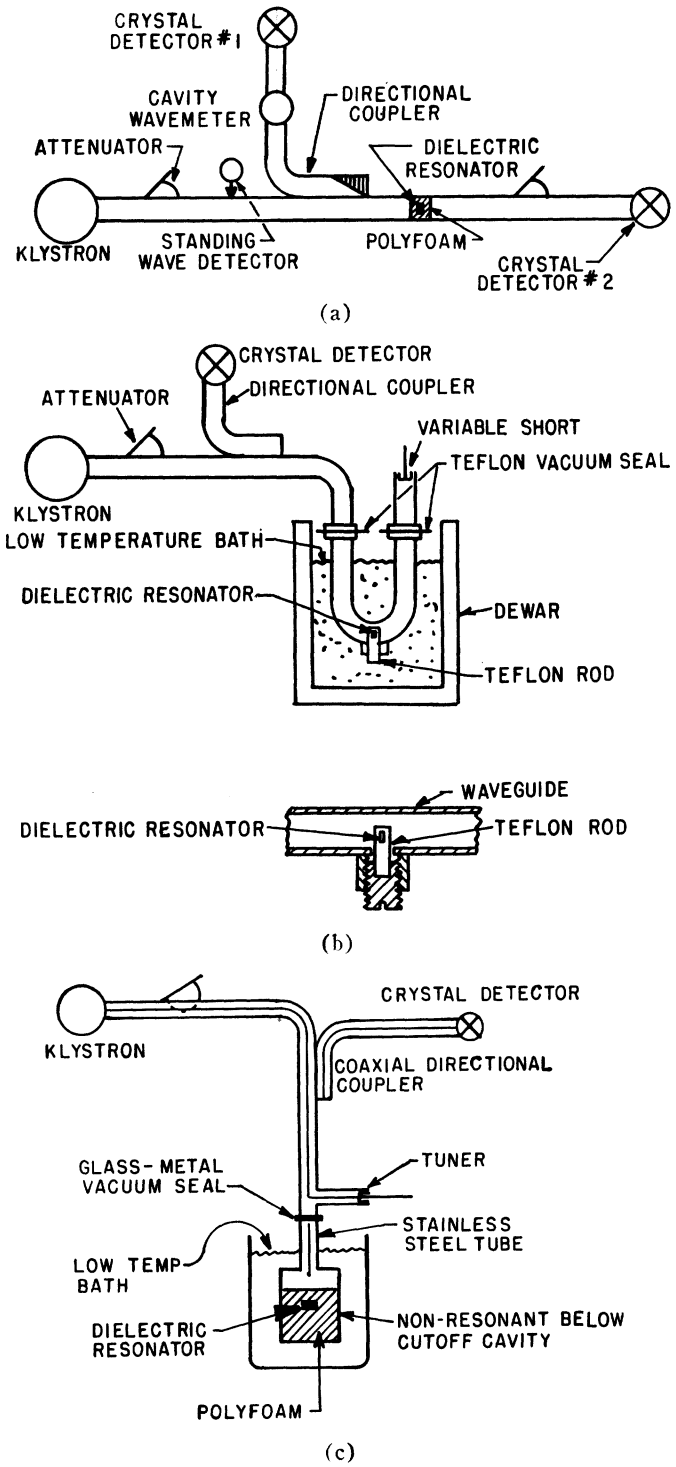

Fig. 5—(a) Microwave set-up for characteristics measurements. (b) Microwave set-up for temperature effect measurements. (c) Microwave set-up for temperature effect measurements.

$\pm 1.5°$ and annealed in an air oven at about 700°C for half an hour. Usually this annealing was quite effective in increasing the Q values. Quite often "pure rutile" has shown different Q values from piece to piece because even a small population of vacancies or dislocations influence the Q values. The $SrTiO_3$ resonators were also cut from the optically oriented boules. Even though the local crystal field is nearly cubic, a birefringent effect [4] was observed at room temperature. $SrTiO_3$ resonators showed large natural relaxation characteristics, and their Q values were increased by approximately a factor two, several days after machining.

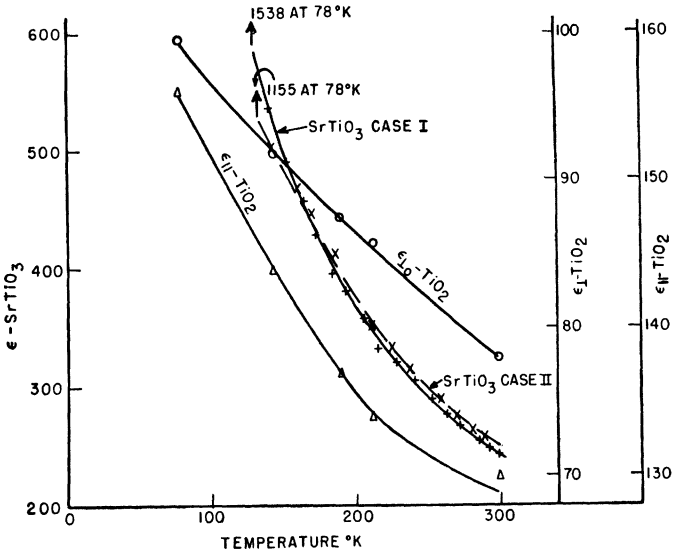

Fig. 6—Temperature vs frequency curve of TiO_2 and $SrTiO_3$.

To compare the theoretical and experimental values the following two experiments were conducted:

a) Accurate measurements of the resonant frequencies were made on accurately finished C band Case I, II and II resonators of size $0.1233'' \times 0.4075'' \times 0.2466'' \pm 0.0003''$. In this case the accuracy of the orientation of the optical axis, referred to the geometrical axis, was better than $\pm 1.5°$.

b) The resonant frequency vs the resonator thickness curve was obtained on X band Case I and II resonators of approximate size $0.20'' \times 0.10'' \times c$.

In experiment a) of the Case I resonator, one can see that the second-order equation (18a) completely agrees with the first-order equation (4) and the boundary equation. Then $\epsilon_\perp$ was obtained from the H-mode frequency, (18a) which depends only upon $\epsilon_\perp$. $\epsilon_\parallel$ was obtained from the E-mode frequency (29a) using $\epsilon_\perp$ and ζ_{i-} values. All twelve measured frequency values agreed with the values calculated by accurate frequency equations using the obtained $\epsilon_\perp$, $\epsilon_\parallel$ and ζ_{i-} constants.

Discrepancies were less than 1 per cent. $\epsilon_\perp$ and $\epsilon_\parallel$ were 78.3 and 127, respectively. These values were also confirmed by applying them to the X band Case I resonators of different frequency and dimensions. The change of $\epsilon_\perp$ and $\epsilon_\parallel$ values between the X and C bands was not noticed. It will be noted that some of the E modes, such as the $E_{11\delta}$, $E_{31\delta}$, and $E_{51\delta}$, were not observed in the experiment. This lack of observation seems to be due to the lack of coupling between the inside and outside resonator fields or to the suppression of these resonance modes by the waveguide field.

The curve obtained from experiment b) of the Case I resonator is shown in Fig. 7. Good agreement of experimental results with the values obtained from the bound-

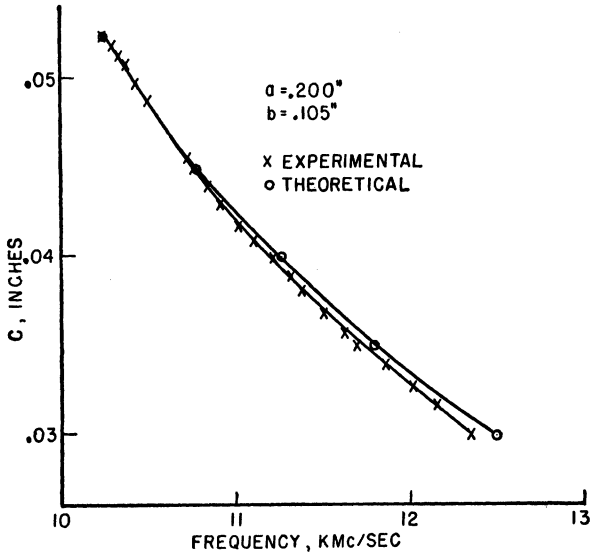

Fig. 7—Thickness vs frequency curve of TiO_2 Case I resonator.

TABLE I
CASE I

Experimental			Theoretical	
Outside field*	Wavelength cm	Q_0(300°K)	Mode	Wavelength cm†
H	9.31	14,000	$H_{11\delta}$	9.31
(E)	(9.31)		($E_{21\delta}$)	(9.31)
H	6.05	16,000	$H_{21\delta}$	6.05
			($E_{31\delta}$)	(6.00)
E	5.24	28,000	$E_{22\delta}$	5.26
E	5.15	5,000	$E_{41\delta}$	5.16
	5.05		$H_{31\delta}$	5.10
E	5.04		E_{212}	4.98
	4.79		$E_{32\delta}$	4.85
	4.77		$H_{12\delta}$	4.75
	4.45		$H_{22\delta}$	4.45
			($E_{51\delta}$)	(4.46)
	4.40		$E_{42\delta}$	4.36
	4.35		$E_{41\delta}$	4.32

* E means electric mode; H means magnetic mode.
† $\epsilon_\perp = 79$, $\epsilon_\parallel = 127$, obtained experimentally, were used.
The dimensions of the crystals are: $a = 0.471$ inch, $b = 0.247$ inch, $c = 0.123$ inch.

ary (26) shows the validity of the assumption of the boundary field on both the E and H modes of Case I resonators (Table I).

The results of experiment a) of the H mode on the much more complicated Cases II and III are listed in Tables II and III. The error at those fundamental modes was 2 per cent.

The curve of experiment b) of the H-fundamental mode of Case II is shown in Fig. 8. This also shows the validity of the boundary and frequency (19) and (20) of this case. On the other hand, the results for the fundamental E mode were not nearly as good as those obtained for the H mode and showed a discrepancy of 20 per cent. The reason for this seems to be the oversimplified boundary field which we used. The effective thickness, $c' = \pi/\zeta_i$ (see Fig. 2), calculated from the boundary equations (25) and (30), is much larger than the c' value which satisfies the experimental results. This

TABLE II
CASE II

Experimental			Theoretical		
Outside field*	Wavelength cm	Q_0(300°K)	Mode	Wavelength cm First-order approx.	Second order approx.
H	8.71		$H_{11\delta}$	7.77	8.53
E	6.86	10,000	$E_{11\delta}$	6.94	
E	6.56	6,000	$E_{21\delta}$	6.75	
H	6.25	16,000	$H_{21\delta}$	6.58	
E	5.90	8,000	$E_{31\delta}$	5.54	
H	5.46	6,000	$H_{22\delta}$	5.13	
H	5.41	18,000	$H_{31\delta}$	5.41	
E	5.14	6,000	E_{212}	5.18	

Mode	E	H
$(\zeta_i/\pi)^2(1/cm^2)$	1.63	4.80

TABLE III
CASE III

Experimental			Theoretical		
Outside field*	Wavelength cm	Q_0(300°K)	Mode	Wavelength cm First-order approx.	Second-order approx.
H	7.35	4,000	$H_{11\delta}$	6.76	7.50
E	6.95	18,000	$E_{11\delta}$	7.94	
E	6.27	10,000	$E_{21\delta}$	6.65	
H	6.17	5,000	$H_{21\delta}$	6.20	
E	5.59	10,000	$E_{31\delta}$	5.46	
H	5.44	4,000	$H_{31\delta}$	5.49	
E	4.97		$E_{21\delta}$	4.98	

Mode	E	E
$(\zeta_i/\pi)^2(1/cm^2)$	1.86	6.51

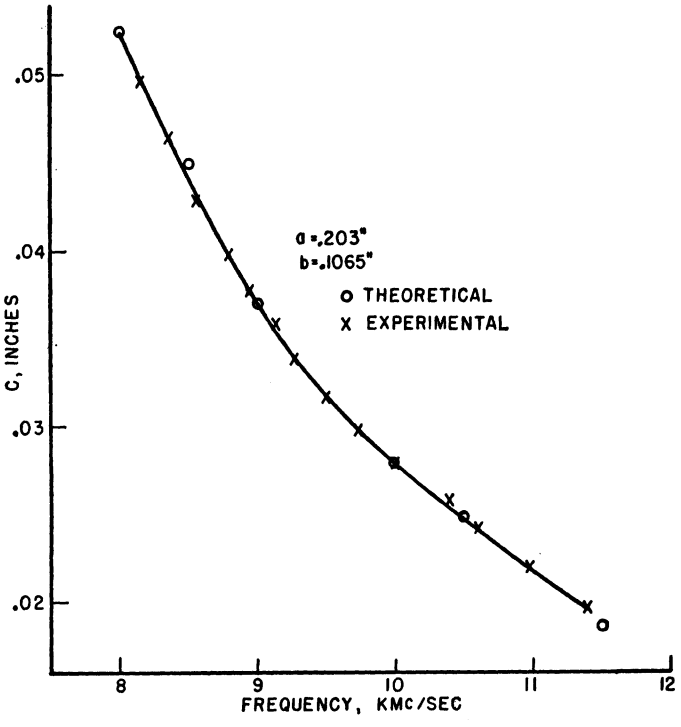

Fig. 8—Thickness vs frequency curve of TiO_2 Case II resonator.

shows that the H field is much more concentrated in the resonator than we assumed.

It should also be noted that these second-order equations are accurate only at a fundamental mode, because the boundary field for high modes can be expected to differ from the field of (27) and (28), except in Case I for which it is nearly true. The modes of high-mode resonances of Cases II and III were identified by the first-order frequency (4).

The constants ζ_{i-}/π for each E and H mode were chosen such that (4) fits the experimental values, especially at higher modes, as explained in Section III.

The modes were also identified by the difference of coupling characteristics between the H and E modes during the measurements. These results are shown in Tables II and III. The mode frequency patterns of all three cases are shown in Fig. 9.

The simpler case of isotropic media, *e.g.*, single crystals of $SrTiO_3$ and KRS-5 (ThBr-ThI), was also examined. The frequency equation for this case for low modes is

$$\left(\frac{2}{\lambda}\right)^2 = \frac{1}{\epsilon}\left[\left(\frac{l}{a}\right)^2 + \left(\frac{m}{b}\right)^2 + \left(\frac{n}{c'}\right)^2\right], \qquad c' = \frac{\pi}{\zeta_i}$$

coupled with the boundary equation

$$\zeta_o = \zeta_i \tan \zeta_i \frac{c'}{2},$$

where

$$(\zeta_o/\pi)^2 = \frac{1}{a^2} + \frac{1}{b^2} - \left(\frac{2}{\lambda}\right)^2.$$

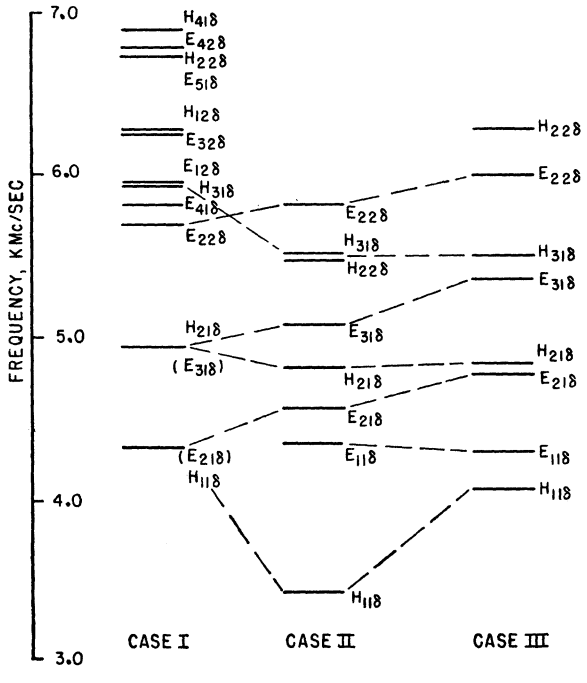

Fig. 9—Mode, frequency pattern of the resonator.

For the higher modes we have

$$\left(\frac{2}{\lambda}\right)^2 = \frac{1}{\epsilon}\left[\left(\frac{l}{a}\right)^2 + \left(\frac{m}{b}\right)^2 + \left(\frac{n}{c}\right)^2\right].$$

The mode behavior of the outside fields was all H type with no exception. This is because the H-pole field couples so much more strongly to the waveguide field than does the E-pole field, as discussed before. The experimentally obtained values at room temperature were

	ϵ	tan δ	Frequency	Manufacturer
$SrTiO_3$	250.0	0.001	8–25 kMc	National Lead Co.
KRS-5	27.5	0.002	4 kMc	Harshaw Chemical Co.

For $SrTiO_3$, ϵ is strongly temperature dependent and also shows a slight, but not negligible, anisotropy at room temperature. This is shown in Fig. 6. There is also a nonlinear power effect at the microwave frequencies [4] at which the measurements were made. An extremely high Q resonance, of the order of one million, was observed in a KRS-5 resonator at X band range in a 1.4°K helium bath.

VIII. Band-Pass and Band-Reject Filters Using Dielectric Resonators

Dielectric resonators can be used as the resonant elements as shown in Fig. 4, simply by placing them in the waveguide at various positions. If a piece of high dielectric constant material, such as rutile, is supported inside a waveguide, a small VSWR, less than 1.3, results for any orientation of the crystal. In the guide size appropriate to low mode resonant frequencies, the crystal at nonresonant frequencies acts merely as a small piece of low-loss insulator. If the crystal is adjusted for critical coupling at resonance, it will absorb all the incident power at resonance, making an absorptive band-reject filter. The crystal can also be adjusted for large mismatches at resonance frequencies, of the order of VSWR equal to 25, such that most of the power is reflected at resonance. In Fig. 4, position A shows maximum coupling for H modes, position B shows maximum coupling for E modes, minimum for H modes, and position C gives intermediate coupling for both. If the crystal is allowed to rest on the waveguide wall as shown in Fig. 4(D), the resonant frequency is changed (see Appendix II) and also, the loss of the waveguide wall at resonance makes Q_o lower. But this is the simplest filter, and the reflection from the resonator is very small.

The Q value of the reject band of the filter is normally of the order of several thousand for rutile at room temperature, but this can be decreased by doping the crystal, reducing it in a hydrogen atmosphere, or by using more than one crystal and stagger tuning. An increase of Q can be achieved by choosing a stress-free crystal or by lowering the temperature of the resonator. The Q and resonant frequency of a resonator of rutile doped

with a paramagnetic salt such as Cr^{3+}, Fe^{3+}, or Mn^{2+} can be changed with an external magnetic field by the electron paramagnetic resonance effect, if the input power is of the order of 0.1 mw, but this requires low temperature operation (78°K).

A type of band-pass filter is illustrated in Fig. 10. Sections of crossed input and output rectangular waveguides are tapered to a short section of a square waveguide. The crystal, in a polyfoam support, is placed along a diagonal of the square section so as to achieve critical coupling to both input and output guides at resonance. The radiation field of the resonator is symmetric along the diagonal of the square waveguide and, hence, couples to both input and output equally. The coupling was adjusted by rotating and moving the crystal along the diagonal. A piece of attenuator card is placed in the output section, as shown, to absorb the incident power-off resonance. One such filter roughly constructed at X band transmitted 60 per cent of the incident power at a resonance of $Q=10{,}000$ with a VSWR no worse than 1.1 anywhere. Off resonance the transmitted power was down at least 35 db. These figures could easily be improved by careful adjustment.

Appendix I

Maxwell's equations,

$$\nabla \times \boldsymbol{E} \equiv -\mu \dot{\boldsymbol{H}}, \qquad \nabla \times \boldsymbol{H} = \epsilon \dot{\boldsymbol{E}}, \tag{32}$$

will be solved for the case in which μ and ϵ are anisotropic, diagonal tensors. The solutions are assumed to be of the following forms:

$$H_x = h_x \begin{matrix}\sin\\ \cos\end{matrix} \xi x \begin{matrix}\sin\\ \cos\end{matrix} \eta y \begin{matrix}\cos\\ \sin\end{matrix} \zeta z e^{i\omega t},$$

$$H_y = h_y \begin{matrix}\cos\\ \sin\end{matrix} \xi x \begin{matrix}\cos\\ \sin\end{matrix} \eta y \begin{matrix}\cos\\ \sin\end{matrix} \zeta z e^{i\omega t},$$

$$H_z = h_z \begin{matrix}\cos\\ \sin\end{matrix} \xi x \begin{matrix}\sin\\ \cos\end{matrix} \eta y \begin{matrix}\sin\\ \cos\end{matrix} \zeta z e^{i\omega t}. \tag{33}$$

The same sort of equations and solutions can be derived for the E field.

From the condition that the determinant obtained from (32) and (33) must be equated to zero for a solution to exist, the following frequency equation is obtained.

$$\left(\frac{2}{\lambda}\right)^2 = \left(\frac{1}{a}\right)^2\left(\frac{1}{\mu_y\epsilon_z}+\frac{1}{\mu_z\epsilon_y}\right)^2+\left(\frac{1}{c}\right)\left(\frac{1}{\mu_x\epsilon_z}+\frac{1}{\mu_z\epsilon_x}\right)+\left(\frac{1}{b}\right)^2\left(\frac{1}{\mu_x\epsilon_y}+\frac{1}{\mu_y\epsilon_x}\right)$$

$$\pm\frac{1}{2}\left[\left(\frac{1}{a}\right)^4\left(\frac{1}{\mu_y\epsilon_z}-\frac{1}{\mu_z\epsilon_y}\right)^2+\left(\frac{1}{c}\right)^4\left(\frac{1}{\mu_z\epsilon_x}-\frac{1}{\mu_x\epsilon_z}\right)^2+\left(\frac{1}{b}\right)^4\left(\frac{1}{\mu_y\epsilon_x}-\frac{1}{\mu_x\epsilon_y}\right)^2\right.$$

$$+2\left(\frac{1}{a}\right)^2\left(\frac{1}{c}\right)^2\left(\frac{1}{\mu_z\epsilon_x}-\frac{1}{\mu_x\epsilon_z}\right)\left(\frac{1}{\mu_z\epsilon_y}-\frac{1}{\mu_y\epsilon_z}\right)+2\left(\frac{1}{a}\right)^2\left(\frac{1}{b}\right)^2\left(\frac{1}{\mu_y\epsilon_x}-\frac{1}{\mu_x\epsilon_y}\right)$$

$$\left.\times\left(\frac{1}{\mu_y\epsilon_z}-\frac{1}{\mu_z\epsilon_y}\right)+2\left(\frac{1}{c}\right)^2\left(\frac{1}{b}\right)^2\left(\frac{1}{\mu_z\epsilon_x}-\frac{1}{\mu_x\epsilon_z}\right)\left(\frac{1}{\mu_y\epsilon_x}-\frac{1}{\mu_x\epsilon_y}\right)\right]^{1/2}.$$

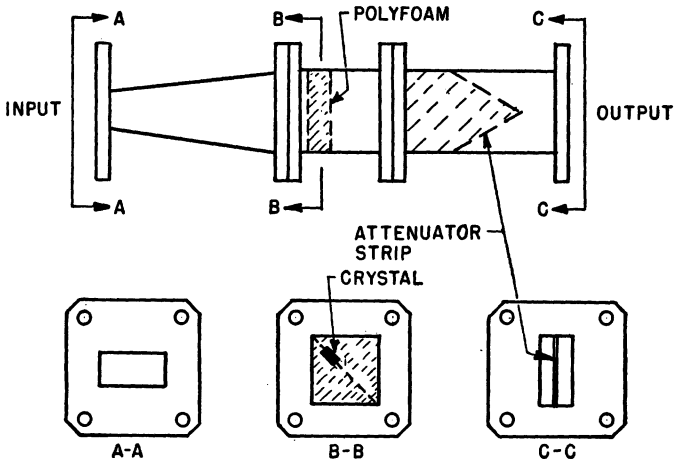

Fig. 10—Band-pass filter.

Here a, b, and c are the resonator dimensions along the x, y, and z directions, respectively. The same result was obtained from the equation of the E field. This is the zero-order solution, and it is assumed that the surface of the resonator coincided with the node or antinode of the field. Its limitations are discussed in the main article.

Appendix II

The Effect of a Metal Wall on a Dielectric Resonator

The effect of a metal wall on a dielectric resonator can be solved readily only for an isotropic, spherical resonator in a concentric metal sphere. This work was done by J. A. Giordmaine [10], and the results are shown in Fig. 11. One can see from Fig. 11 that, if the distance

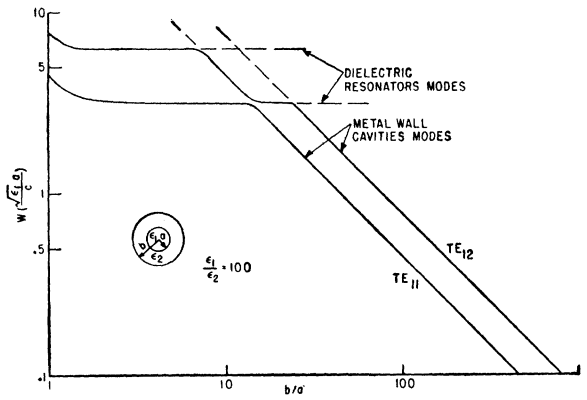

Fig. 11—The effect of a metal wall on the dielectric resonator.

between the surface of a cavity and a dielectric sphere is small, the resonant frequency of the dielectric sphere is influenced by the metal wall. However, if the gap between them becomes larger than a certain value, the dielectric sphere behaves as an independent resonator and has a constant frequency. If the resonant frequencies of two resonators are nearly the same, interference becomes significant and their frequencies shift by an amount proportional to the ratio ϵ_2/ϵ_1. Hence, the clear separation between the dielectric resonator modes and metal-cavity modes can be seen for large ratios of ϵ_1/ϵ_2. If this ratio is extremely large, the interaction is much smaller and the intersection of the mode lines becomes nearly a point.

Similar considerations would hold for rectangular dielectric resonators in a rectangular waveguide, although the results cannot be as readily calculated as in the spherical case.

Acknowledgment

The authors wish to thank Prof. C. H. Townes for his encouragement and the members of the Columbia Radiation Laboratory for useful discussions. We are also thankful to A. Marshall, whose assistance was indispensable in preparing the samples.

References

[1] A. Okaya, *et al.*, Columbia Radiation Lab. Quart. Rept., Columbia University, New York, N. Y.; March 16–June 15, 1959 (unpublished), June 16–September 15, 1959 (unpublished), September 16–December 15, 1959 (unpublished).
[2] R. D. Richtmyer, "Dielectric resonator," *J. Appl. Phys.*, vol. 10, pp. 391–398; June, 1939.
[3] D. Carter and A. Okaya, "Electron paramagnetic of Fe^{3+} in $Ti O_2$ (Rutile)," *Phys. Rev.*, vol. 118, pp. 1485–1490; 1960.
[4] A. Okaya (to be published).
[5] D. Carter, "A CW solid state push-pull maser in the 5 to 6 millimeter wavelength region," *J. Appl. Phys.*, vol. 32, pp. 2541–2542; December, 1961.
[6] S. Foner and L. R. Momo, "CW millimeter wave maser using Fe^{3+} in TiO_2," *J. Appl. Phys.*, vol. 31, pp. 742–743; April, 1960.
[7] H. J. Gerritson and H. R. Lewis, "Operation of a Chromium-Doped Titania Maser at X,K Band." In "Quantum Electronics," C. H. Townes, Ed., Columbia University Press, New York, N. Y., p. 385; 1960.
[8] S. A. Schelkunoff, "Electromagnetic Waves," D. Van Nostrand Co., Inc., New York, N. Y., p. 86; 1943.
[9] J. A. Stratton, "Electromagnetic Theory," McGraw-Hill Book Co., Inc., New York, N. Y., p. 438; 1941.
[10] J. A. Giordmaine (to be published).
[11] A. Okaya, "The rutile microwave resonator," PROC. IRE (*Correspondence*), vol. 48, p. 1921; November, 1960.
[12] A. Okaya, "Electromagnetic Field Expansion in the Dielectric Resonator" (to be published).

CORRECTION

J. Ralph Johler, author of "Propagation of the Low-Frequency Radio Signal," which appeared on pages 404–427 of the April, 1962, issue of PROCEEDINGS, has called the following to the attention of the *Editor*.

On page 408, the line immediately after (31) should read:

"where $\tau=\tau_s$ comprises the special roots of the differential equation of Riccati, noted by Bremmer . . . ."

On page 411, (42) should read:

$$-\operatorname{Im} F_s(t) = \operatorname{Re} i \exp(-\nu t)$$
$$= \exp(-c_1 t)\sin \omega_c t \qquad (0 < t < \infty)$$
$$= 0 \qquad (t < 0).$$

On page 415, the second term of (57) should read:

$$\frac{-i}{4}\exp(-\nu_1 t).$$